International Journal of Mechanical, Industrial and Aerospace Sciences
ISSN: 2517-9950
Vol:13, No:7, 2019

Free Vibration and Buckling of Rectangular Plates under Nonuniform In-Plane Edge Shear Loads

T. H. Young, Y. J. Tsai

***Abstract*—**A method for determining the stress distribution of a rectangular plate subjected to two pairs of arbitrarily distributed in-plane edge shear loads is proposed, and the free vibration and buckling of such a rectangular plate are investigated in this work. The method utilizes two stress functions to synthesize the stress-resultant field of the plate with each of the stress functions satisfying the biharmonic compatibility equation. The sum of stress-resultant fields due to these two stress functions satisfies the boundary conditions at the edges of the plate, from which these two stress functions are determined. Then, the free vibration and buckling of the rectangular plate are investigated by the Galerkin method. Numerical results obtained by this work are compared with those appeared in the literature, and good agreements are observed.

***Keywords*—**Stress analysis, free vibration, plate buckling, nonuniform in-plane edge shear.

I. Introduction

THE problems concerning plate structures subjected to in-plane loads are frequently encountered in structural engineering. The behaviors of free vibration and elastic stability of such plates are primary considerations for structural engineers. Therefore, lots of references about these topics can be found in the literature [1].

References on free vibration and elastic stability of plates subjected to uniform in-plane loads appeared several decades ago. Recent researches on these topics focus mainly on plates subjected to nonuniform in-plane loads. For rectangular plates subjected to nonuniform in-plane edge loads, the stress distribution of the plate must usually be found first before one can tackle the free vibration and elastic stability problems. Tahan et al. [2], [3] utilized single Fourier series solutions to study stress distributions of rectangular plates subjected to in-plane collinear compression.

Kang and Leissa [4] found exact solutions for buckling of rectangular plates having linearly varying in-plane loading on two opposite simply supported edges. In such cases, the stress distribution of the plate is exactly the same as the applied in-plane edge loading. By assuming the transverse displacement to vary sinusoidal in x, the governing partial differential equation of motion is reduced to an ordinary differential equation in y with variable coefficients, for which an exact solution is obtained as a power series by the method of Frobenius. Civalek et al. [5] adopted discrete singular convolution approach to solve the same problem as Kang and Leissa did. Lopatin and Morozov [6] studied buckling of a SSCF rectangular plate subjected to linearly varying loading on two opposite simply-supported edges. The Kantorovich procedure is used to reduce the relevant variational buckling equation to a one-dimensional form, and the equation is then solved by the generalized Galerkin method.

Wang et al. [7] analyzed the buckling of rectangular plates under uniaxial cosine-distributed compressive loads on two opposite edges. Both the stress analysis and buckling problems are solved in an approximate way by the differential quadrature method. Jana and Bhaskar [8] studied the buckling of a simply supported rectangular plate due to uniaxial compressive edge loads symmetrically distributed with respect to the mid-points of two opposite edges. The elasticity solution for the internal in-plane stress field is obtained rigorously using a superposition of Airy's stress functions, and the buckling loads are obtained by Galerkin's method. Buckling loads of composite rectangular plates subjected to nonuniform in-plane loads were presented by Panda and Ramachandra [9]. First the plane elasticity problem is solved to evaluate the approximate stress distribution by the principle of minimum strain energy, and the critical buckling load is obtained using Galerkin's method. Tang and Wang [10] investigated the buckling of symmetrically laminated rectangular plate under parabolic compressions on two opposite edges. Both the stress analysis and buckling problems are solved by the Rayleigh-Ritz approximation method with trial functions used being Chebyshev polynomials multiplying with functions that satisfy either simply-supported or clamped boundary condition along four edges.

Liu and Pavlovic [11] presented an analytical approach for the buckling of simply supported rectangular plates under arbitrary edge loads. Exact solutions for the in-plane stresses are obtained by breaking down the applied edge loads into parts which are able to take advantage of the existing solutions, and the buckling problem is then solved by the Ritz method. Ikhenazen et al. [12] investigated the buckling of simply supported rectangular plates subjected to uniaxial patch compression. Exact stress distribution from existing literature is used, and the finite element method is adopted to find the buckling load of the plate.

Wang et al. [13] investigated the free vibration and buckling of an SCSC rectangular plate under linearly varying in-plane stresses by the differential quadrature method. Srivastava et al. [14] studied the buckling and free vibration of stiffened plates subjected to in-plane partial and concentrated edge loadings. Both the stress analysis and buckling problems

T. H. Young is with the National Taiwan University of Science and Technology, Taipei 10607, Taiwan (corresponding author, e-mail: thyoung@mail.ntust.edu.tw).

Y. G. Tsai is with the National Taiwan University of Science and Technology, Taipei 10607, Taiwan (e-mail: M10103117@mail.ntust.edu.tw).

are solved using the finite element method.

All the above mentioned references consider compressive loads along. Only few references deal with plates subjected to shear loads. Dickinson [15] used the Rayleigh-Ritz method to study the free vibration problem of a simply supported rectangular plate subjected to uniform in-plane shear loads on all edges, and critical buckling loads of the plate are obtained also as the natural frequencies become zero. Recently, the free vibration and buckling problems of simply supported rectangular plates subjected to uniform in-plane shear on all edges, or to uniform compression on two opposite edges and uniform shear on all edges were adopted as benchmark test problems for various finite difference, finite element or finite strip methods [16]-[19].

To author's knowledge, the free vibration and buckling problems of a rectangular plate subjected to nonuniform in-plane edge shear loads, which need a preceding stress analysis, have not been studied yet. Therefore, the stress analysis of a rectangular plate subjected to two pairs of arbitrarily distributed in-plane edge shear loads is carried out first in this work. Once the stress-resultant distribution of the rectangular plate is calculated, the Galerkin method is then adopted to study the free vibration and bucking of the rectangular plate analytically.

II. Equation of Motion

Consider a rectangular plate of dimension $a \times b$ subjected to two pairs of arbitrary distributed in-plane shear loads f(y) and g(x) on two pairs of opposite edges of the plate, as shown in Fig. 1. Due to static equilibrium, these two pairs of edge shear loads must satisfy the following moment equilibrium equation,

$$b\int_0^a g(x)dx = a\int_0^b f(y)dy \tag{1}$$

For lateral dynamic problems, the equation of motion of such a plate in terms of the transverse displacement *w* is given by [1]

$$\rho h\frac{\partial^2 w}{\partial t^2} + D\nabla^4 w = N_{xx}\frac{\partial^2 w}{\partial x^2} + 2N_{xy}\frac{\partial^2 w}{\partial x\partial y} + N_{yy}\frac{\partial^2 w}{\partial y^2} \tag{2}$$

where ρ and h are the mass density and thickness of the plate, respectively. N_{xx} , N_{yy} and N_{xy} are the in-plane stress resultants of the plate. *D* is the flexural rigidity of the plate, and ∇^4 is the biharmonic operator in Cartesian coordinates,

$$D = \frac{Eh^3}{12(1-\upsilon^2)}, \quad \nabla^4 = \frac{\partial^4}{\partial x^4} + 2\frac{\partial^4}{\partial x^2\partial y^2} + \frac{\partial^4}{\partial y^4},$$

in which E and υ are the Young's modulus and the Poisson's ratio of the plate, respectively.

To solve the equation, the in-plane stress resultants N_{xx}, N_{yy} and N_{xy} must be known in advance. If the plate is subjected to uniform in-plane shear loads N_0 on all four edges, these in-plane stress resultants are the same as the applied edge loads, i.e., N_{xx}=N_{yy}=0, and N_{xy}=N_0. If the plate is subjected to non-uniform in-plane edge shear loads, a stress analysis has to carry out to determine the stress-resultant distribution on the plate. First expand the edge shear loads f(y) and g(x) into Fourier cosine series as

$$f(y) = f_0 + \sum_{k=1}^{\infty} f_k \cos\frac{k\pi y}{b}, \tag{3a}$$

$$g(x) = g_0 + \sum_{k=1}^{\infty} g_k \cos\frac{k\pi x}{a}, \tag{3b}$$

where f_k and g_k are Fourier coefficients. Note that f_0 and g_0 are the averages of f(y) and g(x), respectively, and $f_0 = g_0$ is obtained due to moment equilibrium, (1). The edge shear loads can be viewed as the sum of a uniform part f_0 (or g_0) and a nonuniform part represented by the series $\sum_{k=1}^{\infty} f_k \cos\frac{k\pi y}{b}$ (or $\sum_{k=1}^{\infty} g_k \cos\frac{k\pi x}{a}$). Thus, the stress-resultant distribution on the plate due to these two pairs of in-plane edge shear loads can be regarded as a uniformly distributed stress-resultant field N_{xx1}=N_{yy1}=0, and $N_{xy1} = f_0 (= g_0)$ due to the uniform parts of f(y) and g(x) superimposed on a nonuniformly distributed stress-resultant field, N_{xx2} N_{yy2} and N_{xy2} , due to the nonuniform parts of f(y) and g(x) . This nonuniformly distributed stress-resultant field must satisfy the following boundary conditions at the edges of the plate,

$$N_{xx2}|_{x=0,a} = 0, \text{ and } N_{xy2}|_{x=0,a} = \sum_{k=1}^{\infty} f_k \cos\frac{k\pi y}{b}\ , \tag{4a}$$

$$N_{yy2}|_{y=0,b} = 0, \text{ and } N_{xy2}|_{y=0,b} = \sum_{k=1}^{\infty} g_k \cos\frac{k\pi x}{a}\ . \tag{4b}$$

To find this nonuniformly distributed stress-resultant field due to the nonuniform parts of f(y) and g(x), consider two stress functions Φ_1 and Φ_2 which synthesis this nonuniformly distributed stress-resultant field. The stress functions and the in-plane stress resultants are related by

$$N_{xx2i} = \frac{\partial^2\Phi_i}{\partial y^2},\ N_{yy2i} = \frac{\partial^2\Phi_i}{\partial x^2}, \text{ and } N_{xy2i} = \frac{\partial^2\Phi_i}{\partial x\partial y},\quad i = 1 \text{ and } 2. \tag{5}$$

Each of these two stress functions must satisfy the biharmonic compatibility equation, and the sum of the two stress-resultant fields due to these two stress functions must satisfy the above boundary conditions at the edges of the plate. Assume that these two stress functions Φ_1 and Φ_2 can be expressed as Fourier sine series as

$$\Phi_1(x,y) = \sum_{m=1}^{\infty} \varphi_m(x)\sin\frac{m\pi y}{b}, \tag{6a}$$

$$\Phi_2(x,y) = \sum_{n=1}^{\infty} \psi_n(y)\sin\frac{n\pi x}{a}, \tag{6b}$$

where φ_m and ψ_m are Fourier coefficients. Substituting Φ_1 and Φ_2 in (6) into the biharmonic compatibility equation yields

$$\varphi_m(x) = A_m\cosh\frac{m\pi x}{b} + B_m\sinh\frac{m\pi x}{b} + C_m x\cosh\frac{m\pi x}{b} + D_m x\sinh\frac{m\pi x}{b} \tag{7a}$$

$$\psi_n(y) = E_n\cosh\frac{n\pi y}{a} + F_n\sinh\frac{n\pi y}{a} + G_n y\cosh\frac{n\pi y}{a} + H_n y\sinh\frac{n\pi y}{a} \tag{7b}$$

where A_m, B_m, C_m, D_m, E_n, F_n, G_n and H_n are the undermined coefficients to be determined by the boundary conditions in (4). The two stress-resultant fields due to these two stress functions are obtained from the relations between stress-resultants and stress function, as given in the appendix. The nonuniformly distributed stress-resultant field due to the nonuniform parts of f(y) and g(x) is the sum of these two stress-resultant fields.

Substituting N_{xx21}, N_{xx22}, N_{yy21} and N_{yy22} into the corresponding boundary conditions in (4) yields

$$A_m = 0, \text{ and } D_m = -\frac{1}{a}B_m - C_m \coth\frac{m\pi a}{b}, \quad \text{for m} = 1, 2, \ldots \tag{8a}$$

$$E_n = 0, \text{ and } H_n = -\frac{1}{b}F_n - G_n \coth\frac{n\pi b}{a}, \quad \text{for n} = 1, 2, \ldots \tag{8b}$$

The sum of N_{xy21} and N_{xy22} has to satisfy the boundary conditions in (4) also. Since the nonuniform parts of the edge shear loads are expressed in cosine series in (4), and shear stress-resultant distributions on plate edges $N_{xy21}|_{x=0}$, $N_{xy21}|_{x=a}$, $N_{xy22}|_{y=0}$ and $N_{xy22}|_{y=b}$ are also in the forms of cosine series, expand $N_{xy21}|_{y=0}$, $N_{xy21}|_{y=b}$, $N_{xy22}|_{x=0}$ and $N_{xy22}|_{x=a}$ into Fourier cosine series as following,

$$N_{xy21}|_{y=0} = h_{10} + \sum_{k=1}^{\infty} h_{1k} \cos\frac{k\pi x}{a}, \tag{9a}$$

$$N_{xy21}|_{y=b} = h_{20} + \sum_{k=1}^{\infty} h_{2k} \cos\frac{k\pi x}{a}, \tag{9b}$$

$$N_{xy22}|_{x=0} = e_{10} + \sum_{k=1}^{\infty} e_{1k} \cos\frac{k\pi y}{b}, \tag{9c}$$

$$N_{xy22}|_{x=a} = e_{20} + \sum_{k=1}^{\infty} e_{2k} \cos\frac{k\pi y}{b}, \tag{9d}$$

where h_{1k}, h_{2k}, e_{1k} and e_{2k} are Fourier coefficients. Note that $h_{10} = h_{20} = e_{10} = e_{20} = 0$ since they represent the averages of $N_{xy21}|_{y=0}$, $N_{xy21}|_{y=b}$, $N_{xy22}|_{x=0}$ and $N_{xy22}|_{x=a}$, and the averages of N_{xy21} and N_{xy22} vanish on the corresponding edges of the plate. Expressions of h_{1k}, h_{2k}, e_{1k} and e_{2k} are given in the appendix. Substituting N_{xy21} and N_{xy22} into the corresponding boundary conditions in (4) yields

$$h_{1k} - \left[\left(\frac{k\pi}{a}\right)^2 F_k + \frac{k\pi}{a} G_k\right] = g_k, \tag{10a}$$

$$h_{2k} + \left[\frac{k\pi}{ab}\sinh\frac{k\pi b}{a} F_k + \left(\frac{k\pi}{a}\right)^2 \frac{b}{\sinh\frac{k\pi b}{a}} G_k\right] = g_k, \tag{10b}$$

$$e_{1k} - \left[\left(\frac{k\pi}{b}\right)^2 B_k + \frac{k\pi}{b} C_k\right] = f_k, \tag{10c}$$

$$e_{2k} + \left[\frac{k\pi}{ab}\sinh\frac{k\pi a}{b} B_k + \left(\frac{k\pi}{b}\right)^2 \frac{a}{\sinh\frac{k\pi a}{b}} C_k\right] = f_k, \text{ k} = 1, 2, \ldots \tag{10d}$$

Since h_{1k}, h_{2k}, e_{1k} and e_{2k} are functions of B_k, C_k, F_k and G_k, the above equation can be expressed in matrix form as

$$[K_i]\boldsymbol{X} = \boldsymbol{F} \tag{11}$$

where $[K_i]$ is the in-plane stiffness matrix of the plate; column matrix $\boldsymbol{X}$ is formed by all B_k, C_k, F_k and G_k, and column matrix $\boldsymbol{F}$ is formed by all f_k and g_k. Solving (11) for all B_k, C_k, F_k and G_k, the nonuniformly distributed stress-resultant field due to the nonuniform parts of f(y) and g(x) is determined by summing up the stress-resultant fields due to the stress functions Φ_1 and Φ_2. Imposing the previously mentioned uniformly distributed stress-resultant field on it, the in-plane stress resultants N_{xx}, N_{yy} and N_{xy} of the plate due to these two pairs of in-plane edge shear loads are obtained.

Once the stress-resultant distribution of the rectangular plate is obtained, the free vibration and bucking of such a rectangular plate are then analyzed by the Galerkin method. Assume the transverse displacement *w* of the plate to have the form,

$$\text{w(x, y, t)} = \sum_{p=1}^{P}\sum_{q=1}^{Q} A_{pq}(t)\phi_{pq}(x, y), \tag{12}$$

where the trial functions $\phi_{pq}(x, y)$ satisfy all lateral boundary conditions of the plate, and P and Q are the numbers of terms used in the x- and y-directions, respectively. $A_{pq}(t)$ are the undetermined functions of time. Substituting the assumed displacement in (12) into the equation of motion in (2) yields a certain residue. Galerkin's method requires that this residue weighted by the trial functions $\phi_{pq}(x, y)$ vanishes over the entire plate, which gives the following discretized equation in time,

$$[\text{M}]\ddot{\mathbf{q}}(t) + \left([\text{K}_\text{o}] + [\text{K}_\text{g}]\right)\mathbf{q}(t) = \mathbf{0}, \tag{13}$$

where [M] is the mass matrix; $[\text{K}_\text{o}]$ and $[\text{K}_\text{g}]$ are the out-of-plane stiffness matrix and the geometric stiffness matrix due to in-plane stress resultants, respectively. **q**(t) is a column matrix formed by all $A_{pq}(t)$. Assume the solution of the discretized equation is of the form $\mathbf{q}(\text{t}) = \mathbf{u}e^{i\omega t}$, where **u** is a constant column matrix, and ω is the natural frequency of the plate; $\text{i} = \sqrt{-1}$. Substituting the assumed solution into the discretized equation renders the following eigenvalue problem,

$$\left([\text{K}_\text{o}] + [\text{K}_\text{g}]\right)\mathbf{u} = \omega^2[\text{M}]\mathbf{u}, \tag{14}$$

Solving this eigenvalue problem gives the natural frequencies ω and the eigenvectors **u**, which are used to calculate the corresponding mode shapes of the plate by using (12). Buckling loads can be obtained as the natural frequencies of the plate become zero, and the mode shapes under these loads are the buckling mode shapes.

III. Numerical Results

In this section, in-plane stress resultants of rectangular plates subjected to two pairs of in-plane shear loads on two pairs of opposite edges are given first by using the method proposed in this work. Fig. 2 shows the in-plane stress resultants N_{xx}, N_{yy} and N_{xy} on the edges of a square plate subjected to a pair of

linear distributed in-plane shear loads on a pair of opposite edges and a pair of parabolic distributed in-plane shear on the others. The shear load on opposite edges x=0 and x=a is $f(y) = 2\,(y/b)f_0$, and the shear load on opposite edges y=0 and y=b is $g(x) = (3/5)[1 + 4(x/a) - 4(x/a)^2]g_0$, as shown in Fig. 2 (a). Remind that $f_0 = g_0$ due to static equilibrium by (1). Figs. 2 (c) and 2 (e) show that both N_{xx} and N_{yy} are identically 0 on the edges $x = 0$ and $y = 0$, respectively, while Figs. 2 (b) and 2 (d) illustrate that N_{xy} is linear varying on the edge $x = 0$ and is parabolic varying on the edge $y = 0$, respectively. The in-plane stress resultants N_{xx}, N_{yy} and N_{xy} on the edges match exactly with the applied edge shear loads except at corners of the plate where small amounts of errors are observed due to Gibb's phenomenon existed in Fourier series expansion of applied edge shear loads.

Fig. 3 depicts the in-plane stress resultants N_{xx}, N_{yy} and N_{xy} of a square plate subjected to concentrated in-plane shear loads F_o at the mid-points of all edges. Both N_{xx} and N_{yy} are anti-symmetrically distributed with respective to plate center in Figs. 3 (c) and 3 (d). Theoretically two zero stress lines should coincide two middle lines of the plate which connect the mid-points of the opposite edges and pass through the plate center, and there will be stress free on all edges of the plate. However, small amounts of errors exist in these two figures owing to truncation errors in Fourier series expansion of applied edge shear loads. Stress concentration is observed at the mid-points of the edges where concentrated in-plane shear load is applied. From Fig. 3 (b), shear stress resultant N_{xy} is symmetrically distributed with respect to two middle lines of the plate, and the shear stress resultants on the inscribe circle and the astroid of the plate are equal to F_0/b. Of course, stress concentration is also observed at the mid-points of the edges.

Fig. 4 presents the in-plane stress resultants N_{xx}, N_{yy} and N_{xy} of a square plate subjected to two pairs of linear distributed in-plane shear loads on two pairs of opposite edges. The shear load on opposite edges x=0 and x=a is $f(y) = 2(y/b)f_0$, and is $g(x) = 2(x/a)g_0$ on the other opposite edges y=0 and y=b, as shown in Fig. 4 (a). Note that $f_0 = g_0$ since a=b. It is observed from Figs. 4 (c) and 4 (d) that both N_{xx} and N_{yy} are anti-symmetrically distributed with respective to plate center. Theoretically, the zero stress line should coincide with one of the diagonals of the square plate, but actually there are small amounts of errors around corners owing to truncation errors in Fourier series expansion of applied edge shear loads. Normal stress resultants N_{xx} and N_{yy} left below this line are compressive, and are tensile right above this line. From Fig. 4 (b), shear stress resultant N_{xy} is symmetrically distributed with respect to one of the diagonals of the square plate, and its values increases from 0 to $2f_0$ roughly along this diagonal from the left bottom corner to the right top corner. The magnitudes of N_{xy} on the other diagonal equal the average of the applied edge shear f_0.

Fig. 5 illustrates the in-plane stress resultants N_{xx}, N_{yy} and N_{xy} of a rectangular plate with aspect ratio $a/b = 3$ subjected to the same linear distributed in-plane shear loads as Fig. 4. Compared with the above figure, similar patterns are observed between the corresponding figures except that these figures are stretched in the longitudinal direction, and zero-stress lines are further distorted into curves in these figures since the plate is not square any more.

As examples of application of the free vibration analysis conducted in this work, only rectangular plates simply-supported all around are considered in numerical result presentation. In these cases, trial functions in the assumed displacement, (12), are taken as

$$\phi_{pq}(x, y) = \sin\frac{p\pi x}{a}\sin\frac{q\pi y}{b}, \tag{15}$$

which satisfy all boundary conditions of the simply-supported plate. Free vibration analyses of rectangular plates with other boundary conditions can be done easily by considering other comparison functions as trial functions.

Before presenting the numerical results of free vibration analysis obtained by this work, verification of the accuracy of the results is carried out first by comparing with those existed in literature. Fig. 6 shows eigenvalue curves ω^2 of rectangular plates subjected to uniformly distributed in-plane edge shear loads. This figure shows the lowest eigenvalue curve of a square plate and the lowest two eigenvalue curves of rectangular plates of aspect ratios $a/b = 1/2$ and $1/3$. It is observed that the curves calculated by this work match completely all curves obtained by Dickinson [15]. All eigenvalue curves lower as the edge shear loads increase. The coordinate values of the points where eigenvalue curves meet the abscissa are buckling loads of the plate. From this figure, the first buckling load of a square plate subjected to uniformly distributed in-plane edge shear loads is $92.166\,D/a^2$, while the first buckling load of a square plate subjected to uniformly distributed in-plane edge compressive loads is $2\pi^2\,D/a^2$ [1]. Therefore, a square plate is much more liable to buckle when subjected to uniformly distributed in-plane edge compressive loads than to uniformly distributed in-plane edge shear loads.

Fig. 7 depicts the lowest eight natural frequency curves of a square plate subjected to four different distributions of in-plane edge shear loads with the same resultants. The distributions of in-plane edge shear loads on all edges range from uniform distribution to trapezoid and finally to triangular distribution by changing their varying rates. The solid curves, dash curves, dot curves and chain curves denote natural frequency curves subjected to uniformly distributed loads and linearly varying loads of varying rates $1/5$, 1 and 2, respectively. For an unloaded square plate, the natural frequencies are $\omega_{mn} = (m^2 + n^2)\pi^2\sqrt{\rho h b^4/D}$, and hence the lowest eight modes in order are (1,1), (1,2) and (2,1), (2,2), (1,3) and (3,1), (2,3) and (3,2) modes. When the distributed in-plane edge shear loads increase, the frequency curves for degenerate modes, such as (1,2) and (2,1) modes, split into two curves - one goes up, and the other goes down, while the frequency curves of the remaining modes lower. The frequency curves of the sixth and seventh modes cross each other without veering. As the distributions of in-plane edge shear loads change from uniform

distribution to triangular distribution, the frequency curves of the first, second, third fifth and sixth modes lower, while the others rise as the varying rate increases. Therefore, the lowest three buckling loads reduce as the distributions of in-plane edge shear loads change from uniform distribution to triangular distribution.

Fig. 8 shows mode shapes of the lowest eight natural modes of a square plate subjected to uniformly distributed in-plane edge shear loads. It is found that the first, fourth and sixth mode shapes are symmetric with respect to both diagonals of the square plate, and the fifth mode shape is anti-symmetric with respect to both diagonals. The second and seventh mode shapes are anti-symmetric with respect to the 45° diagonal and symmetric with respect to the 135° diagonal, while the third and eighth mode shapes have the opposite pattern because of the direction of the applied in-plane edge shear loads. Fig. 9 presents the lowest four buckling mode shapes of a square plate subjected to uniformly distributed in-plane edge shear loads. It is observed that all buckling mode shapes look similar to the corresponding natural mode shapes of the square plate. Therefore, natural mode shapes would not change much as the magnitude of the applied in-plane edge shear loads change.

Fig. 10 depicts the lowest eight natural frequency curves of a square plate subjected to two different locations of concentrated in-plane edge shear loads F_o. The solid curves and the dash curves denote natural frequency curves subjected to concentrated loads at $1/5$ of the edge length and at the mid-points, respectively, on all edges. When the concentrated in-plane edge shear loads increase, the frequency curves for degenerate modes split into two curves - one goes up, and the other goes down, while the frequency curves of the remaining modes lower. The frequency curves of the fourth and fifth modes cross each other without veering. As the application point of concentrated in-plane edge shear loads move from the mid-points to $1/5$ of the edge length, the frequency curves for degenerate modes generally split away further such that the lowest four buckling loads of a square plate subjected to concentrated loads at $1/5$ of the edge length are lower than those subjected to concentrated loads at the mid-points. Furthermore, compared Fig. 10 to Fig. 7, the lowest buckling load of a square plate subjected to concentrated loads at the mid-points is about $1/3$ smaller than that subjected to uniformly distributed loads having the same resultants as the concentrated loads.

Fig. 11 shows mode shapes of the lowest eight natural modes of a square plate subjected to concentrated in-plane edge shear loads at the midpoints of all edges. It is found that except for the fourth mode which is anti-symmetric with respect to the plate center, all other mode shapes are similar to the corresponding ones of a square plate subjected to uniform in-plane edge shear loads. Moreover, the lowest eight buckling mode shapes look similar to the corresponding natural mode shapes of the square plate.

Fig. 12 illustrates the lowest eight natural frequency curves of a rectangular plate of aspect ratio $a/b = 2$ subjected to two different distributions of in-plane edge shear loads with the same resultants. The solid curves and the dash curves denote natural frequency curves subjected to uniformly distributed loads and concentrated loads at mid-points of all edges. For an unloaded rectangular plate of aspect ratio $a/b = 2$, the natural frequencies are $\omega_{mn} = [(mb/a)^2 + n^2]\pi^2\sqrt{\rho h b^4/D}$, and hence the lowest eight modes in order are (1,1), (2,1), (3,1), (1,2), (2,2) and (4,1), (3,2) and (5,1) modes. When the applied in-plane edge shear loads increase, the frequency curves for degenerate modes, i.e., (2,2) and (4,1) modes, split into two curves - one goes up, and the other goes down, while the frequency curves of the remaining modes lower for both uniformly distributed and concentrated loads, except the seventh mode for uniformly distributed loads. The frequency curves for uniformly distributed loads are generally higher than the curves for concentrated loads, and hence the lowest few buckling loads of the rectangular plate for concentrated loads are smaller than those for uniformly distributed loads.

IV. Conclusion

In this work, a procedure to obtain the stress distribution of a rectangular plate subjected to two pairs of arbitrarily distributed in-plane edge shear loads has been demonstrated, and based on the determined stress distribution, free vibration and bucking of such a rectangular plate are investigated. From the obtained numerical results for stress and free vibration analyses, some conclusions are drawn as follows.

1. When a rectangular plate is subjected to two pairs of in-plane shear loads of the same distribution on two pairs of opposite edges, both in-plane normal stress resultants N_{xx} and N_{yy} are anti- symmetrically distributed with respective to plate center, while the in-plane shear stress resultant N_{xy} is symmetrically distributed with respect to one of the diagonals of the square plate, depending on the direction of the applied in-plane edge shear loads.
2. The lowest buckling load of a square plate subjected to concentrated loads at the mid-points is about $1/3$ smaller than that subjected to uniformly distributed loads having the same resultants as the concentrated loads. As the application point of concentrated in-plane edge shear loads move from mid-points to corners, the lowest buckling load further reduces.
3. Natural mode shapes of a square plate would not change much as the magnitude of the applied in-plane edge shear loads change, and all buckling mode shapes look similar to the corresponding natural mode shapes of the square plate.
4. Except for the fourth mode of a square plate subjected to concentrated loads at the mid-points on all edges, all other natural mode shapes are similar to the corresponding ones of a square plate subjected to uniform in-plane edge shear loads.

Appendix

The stress-resultant field due to stress function Φ_1 is

$$N_{xx21}(x,y) = \sum_{m=1}^{\infty} -[A_m \cosh\frac{m\pi x}{b} + B_m \sinh\frac{m\pi x}{b} + C_m\, x\cosh\frac{m\pi x}{b} + D_m\, x\sinh\frac{m\pi x}{b}]\left(\frac{m\pi}{b}\right)^2 \sin\frac{m\pi y}{b}$$

$$N_{yy21}(x,y)=\sum_{m=1}^{\infty}[A_m\left(\frac{m\pi}{b}\right)^2\cosh\frac{m\pi x}{b}+B_m\left(\frac{m\pi}{b}\right)^2\sinh\frac{m\pi x}{b}+2C_m\frac{m\pi}{b}\sinh\frac{m\pi x}{b}+C_m\left(\frac{m\pi}{b}\right)^2 x\cosh\frac{m\pi x}{b}+2D_m\frac{m\pi}{b}\cosh\frac{m\pi x}{b}+D_m\left(\frac{m\pi}{b}\right)^2 x\sinh\frac{m\pi x}{b}]\sin\frac{m\pi y}{b}$$

$$N_{xy21}(x,y)=\sum_{m=1}^{\infty}-[A_m\frac{m\pi}{b}\sinh\frac{m\pi x}{b}+B_m\frac{m\pi}{b}\cosh\frac{m\pi x}{b}+C_m\cosh\frac{m\pi x}{b}+C_m\frac{m\pi}{b}x\sinh\frac{m\pi x}{b}+D_m\sinh\frac{m\pi x}{b}+D_m\frac{m\pi}{b}x\cosh\frac{m\pi x}{b}]\frac{m\pi}{b}\cos\frac{m\pi y}{b}$$

The stress-resultant field due to stress function Φ_2 is

$$N_{xx22}(x,y)=\sum_{n=1}^{\infty}[E_n(\frac{n\pi}{a})^2\cosh\frac{n\pi y}{a}+F_n(\frac{n\pi}{a})^2\sinh\frac{n\pi y}{a}+2G_n\frac{n\pi}{a}\sinh\frac{n\pi y}{a}+G_n(\frac{n\pi}{a})^2 y\cosh\frac{n\pi y}{a}+2H_n\frac{n\pi}{a}\cosh\frac{n\pi y}{a}+H_n(\frac{n\pi}{a})^2 y\sinh\frac{n\pi y}{a}]\sin\frac{n\pi x}{a}$$

$$N_{yy22}(x,y)=\sum_{n=1}^{\infty}-[E_n\cosh\frac{n\pi y}{a}+F_n\sinh\frac{n\pi y}{a}+G_n y\cosh\frac{n\pi y}{a}+H_n y\sinh\frac{n\pi y}{a}](\frac{n\pi}{a})^2\sin\frac{n\pi x}{a}$$

$$N_{xy22}(x,y)=\sum_{n=1}^{\infty}[E_n\frac{n\pi}{a}\sinh\frac{n\pi y}{a}+F_n\frac{n\pi}{a}\cosh\frac{n\pi y}{a}+G_n\cosh\frac{n\pi y}{a}+G_n\frac{n\pi}{a}y\sinh\frac{n\pi y}{a}+H_n\sinh\frac{n\pi y}{a}+H_n\frac{n\pi}{a}y\cosh\frac{n\pi y}{a}]\frac{n\pi}{a}\cos\frac{n\pi x}{a}$$

Fourier coefficients of $N_{xy1}|_{y=0}$, $N_{xy1}|_{y=b}$, $N_{xy2}|_{x=0}$ and $N_{xy2}|_{x=a}$ are

$$h_{1k}=\sum_{m=1}^{\infty}\frac{\frac{4}{a}\left(\frac{m\pi}{b}\right)^2\left(\frac{k\pi}{a}\right)^2}{\left[\left(\frac{m\pi}{b}\right)^2+\left(\frac{k\pi}{a}\right)^2\right]^2}\{\frac{1}{a}\left[\cosh\frac{m\pi a}{b}(-1)^k-1\right]B_m+\frac{(-1)^k-\cosh\frac{m\pi a}{b}}{\sinh\frac{m\pi a}{b}}C_m\}$$

$$h_{2k}=\sum_{m=1}^{\infty}\frac{\frac{4}{a}\left(\frac{m\pi}{b}\right)^2\left(\frac{k\pi}{a}\right)^2(-1)^m}{\left[\left(\frac{m\pi}{b}\right)^2+\left(\frac{k\pi}{a}\right)^2\right]^2}\{\frac{1}{a}[\cosh\frac{m\pi a}{b}(-1)^k-1]B_m+\frac{(-1)^k-\cosh\frac{m\pi a}{b}}{\sinh\frac{m\pi a}{b}}C_m\}$$

$$e_{1k}=\sum_{n=1}^{\infty}\frac{\frac{4}{b}\left(\frac{n\pi}{a}\right)^2\left(\frac{k\pi}{b}\right)^2}{\left[\left(\frac{n\pi}{a}\right)^2+\left(\frac{k\pi}{b}\right)^2\right]^2}\{\frac{1}{b}[\cosh\frac{n\pi b}{a}(-1)^k-1]F_n+\frac{(-1)^k-\cosh\frac{n\pi b}{a}}{\sinh\frac{n\pi b}{a}}G_n\}$$

$$e_{2k}=\sum_{n=1}^{\infty}\frac{\frac{4}{b}\left(\frac{n\pi}{a}\right)^2\left(\frac{k\pi}{b}\right)^2(-1)^n}{\left[\left(\frac{n\pi}{a}\right)^2+\left(\frac{k\pi}{b}\right)^2\right]^2}\{\frac{1}{b}[\cosh\frac{n\pi b}{a}(-1)^k-1]F_n+\frac{(-1)^k-\cosh\frac{n\pi b}{a}}{\sinh\frac{n\pi b}{a}}G_n\}$$

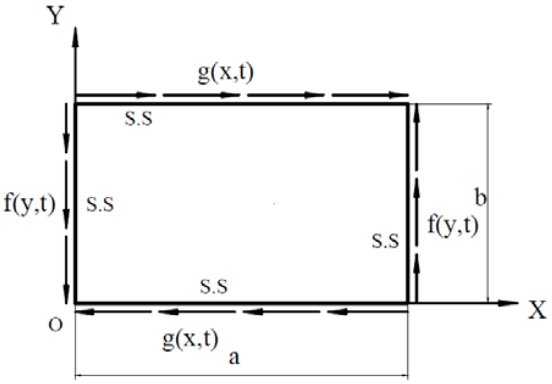

Fig. 1 A simply supported rectangular plate subjected to two pairs of arbitrary distributed in-plane shear loads on two pairs of opposite edges

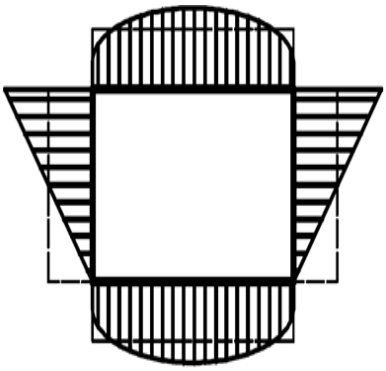

(a) Applied shear loads

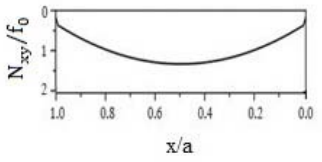

(b) $\frac{x}{a}=0$

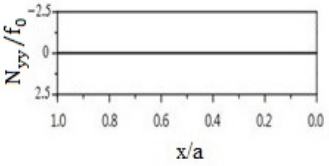

(c) $\frac{x}{a}=0$

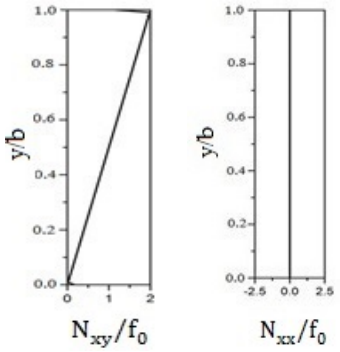

(d) $\frac{y}{b} = 0$ (e) $\frac{y}{b} = 0$

Fig. 2 In-plane stress resultants on the edges of a square plate subjected to a pair of linear distributed in-plane shear on a pair of opposite edges and a pair of parabolic distributed in-plane shear on the others.

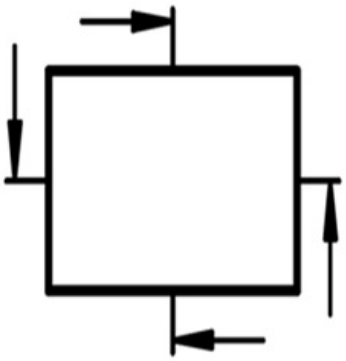

(a) Applied shear loads

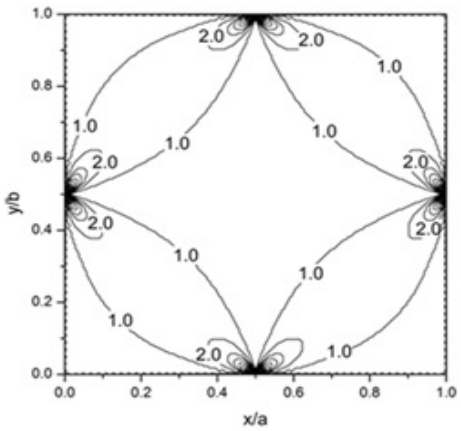

(b) $\frac{N_{xy}\, b^2}{D}$

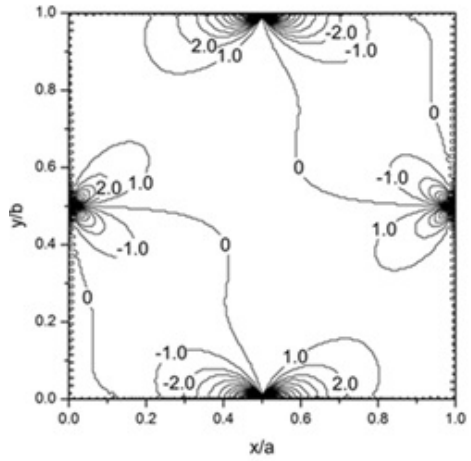

(c) $\frac{N_{xx}\, b^2}{D}$

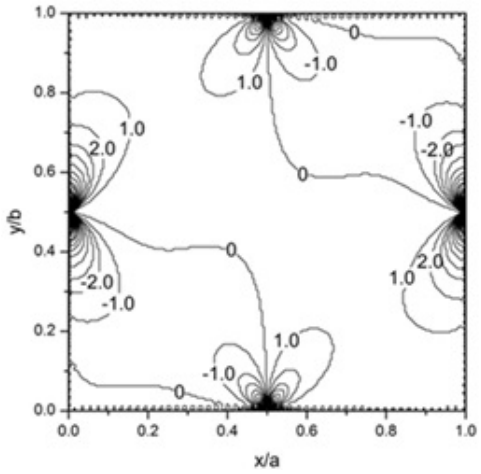

(d) $\frac{N_{yy}\, b^2}{D}$

Fig. 3 In-plane stress resultants of a square plate subjected to concentrated in-plane shear loads F_o at the mid-points of all edges.

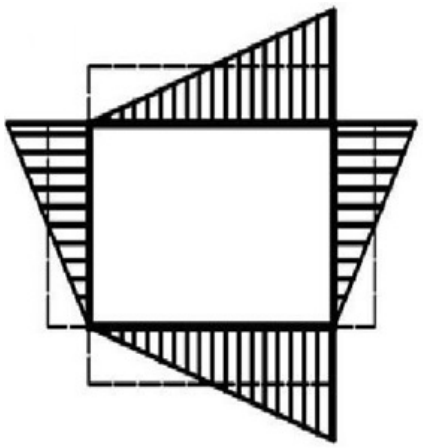

(a) Applied shear loads

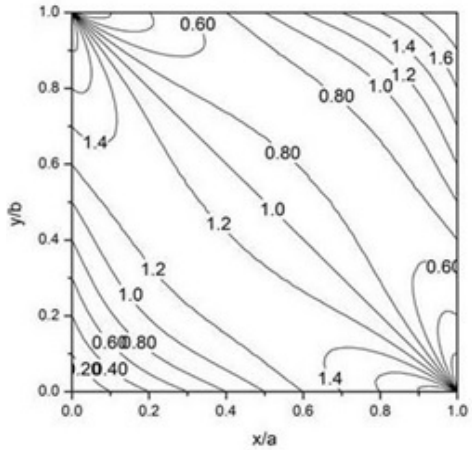

(b) $\frac{N_{xy}\, b^2}{D}$

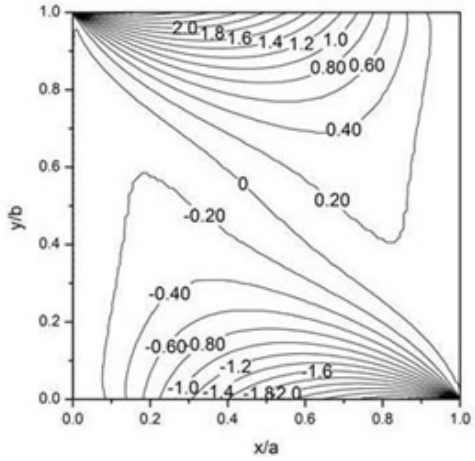

(c) $\frac{N_{xx}\, b^2}{D}$

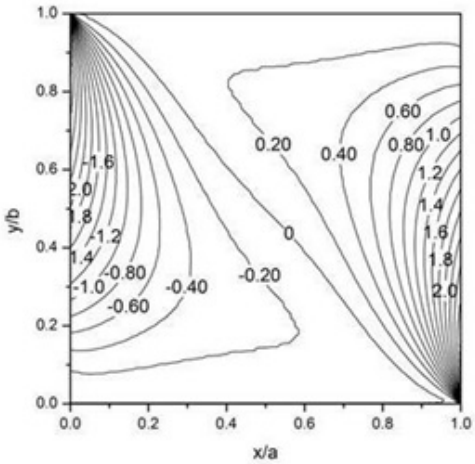

(d) $\frac{N_{yy}\, b^2}{D}$

Fig. 4 In-plane stress resultants of a square plate subjected to two pairs of linear distributed in-plane shear on two pairs of opposite edges

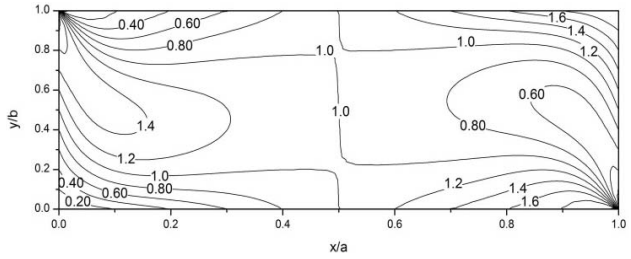

(a) $\frac{N_{xy}b^2}{D}$

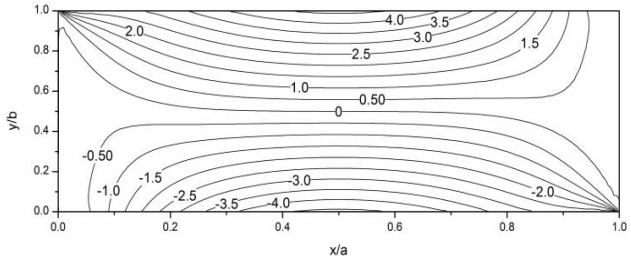

(b) $\frac{N_{xx}b^2}{D}$

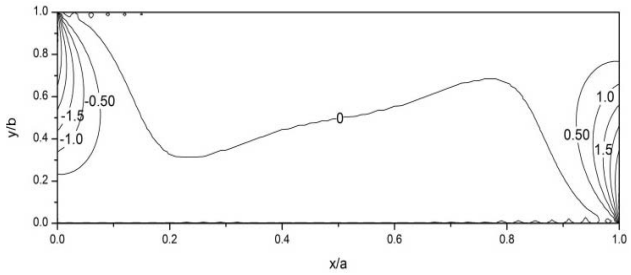

(c) $\frac{N_{yy}b^2}{D}$

Fig. 5 In-plane stress resultants of a rectangular plate with aspect ratio $a/b = 3$ subjected to linear distributed in-plane shear loads on all edges

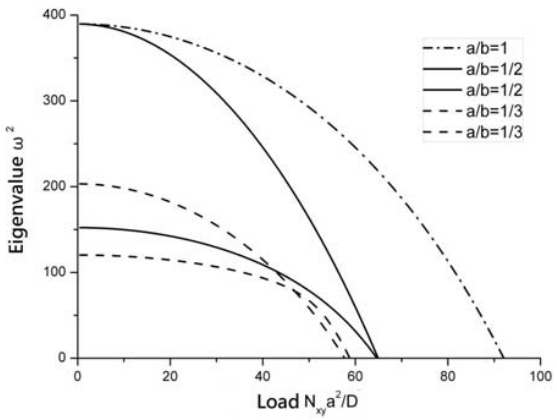

Fig. 6 Eigenvalue curves of rectangular plates subjected to uniformly distributed in-plane edge shear loads N_{xy}

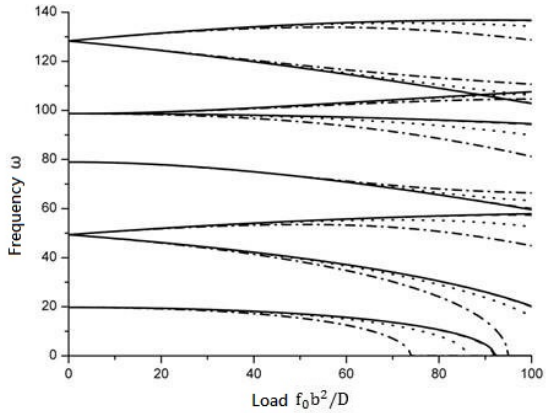

Fig. 7 Lowest eight natural frequency curves of a square plate subjected to four different varying rates of linearly distributed in-plane edge shear loads.

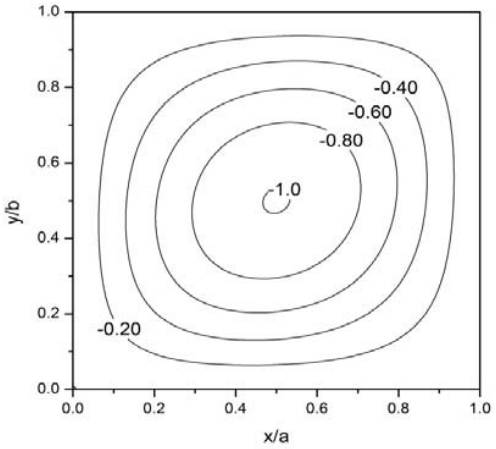

(a) 1st natural mode

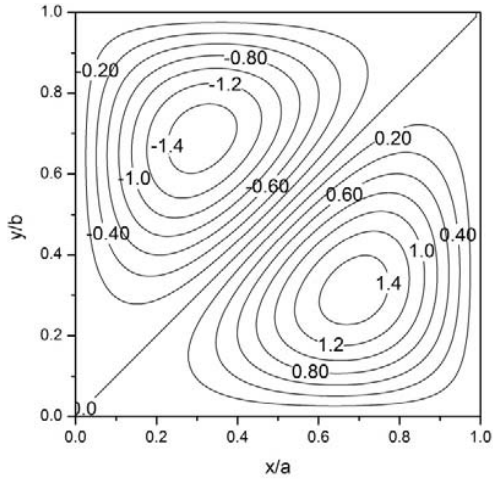

(b) 2nd natural mode

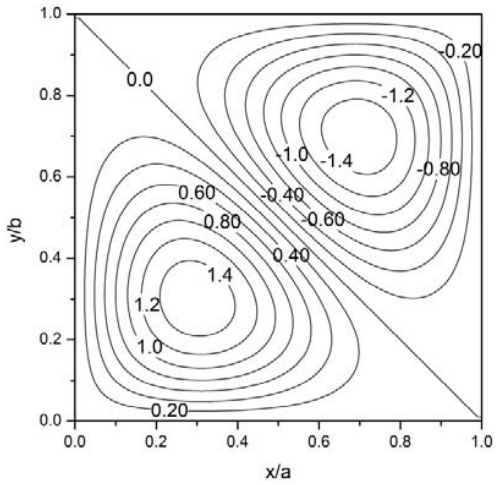

(c) 3rd natural mode

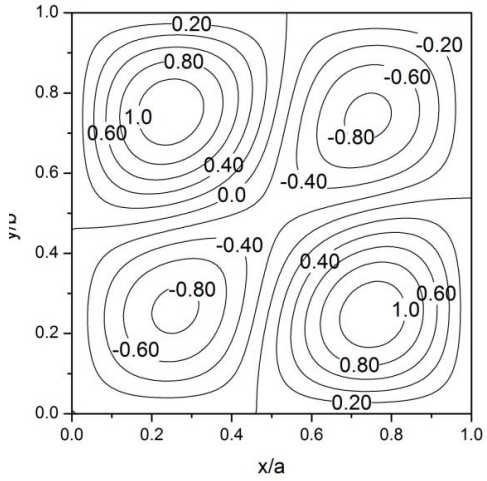

(d) 4th natural mode

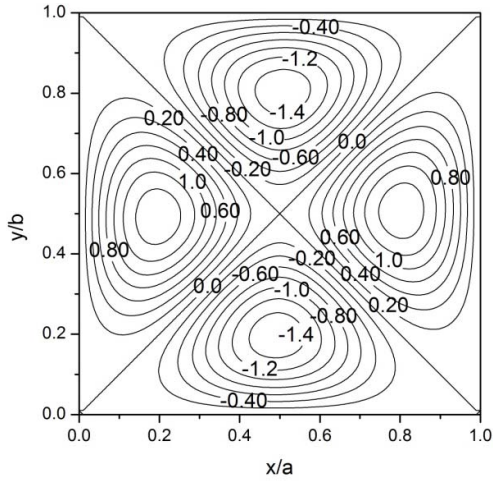

(e) 5th natural mode

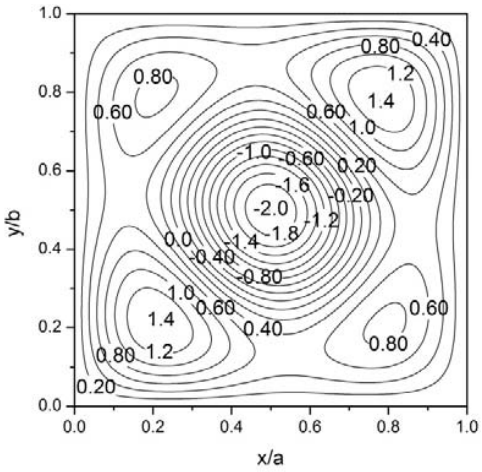

(f) 6th natural mode

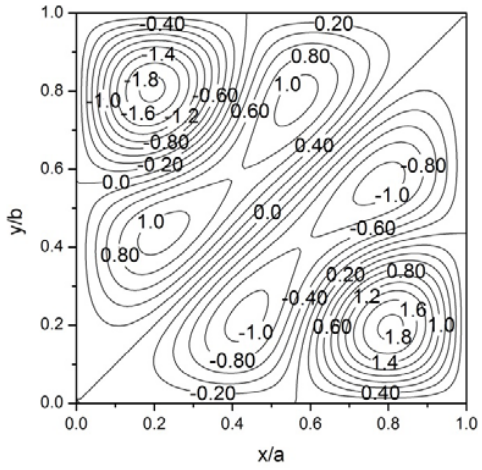

(g) 7th natural mode

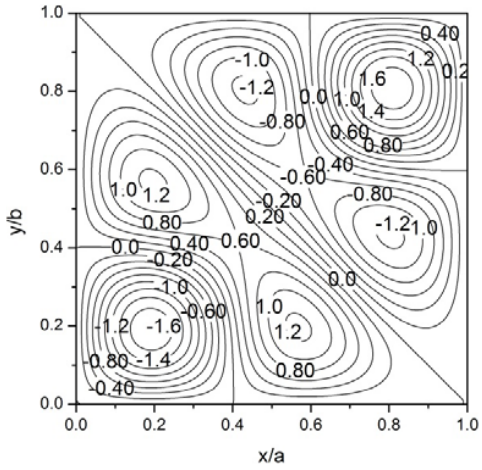

(h) 8th natural mode

Fig. 8 Natural mode shapes of a simply supported square plate subjected to uniformly distributed in-plane edge shear loads N_{xy}. $\frac{N_{xy}\,b^2}{D}$=20

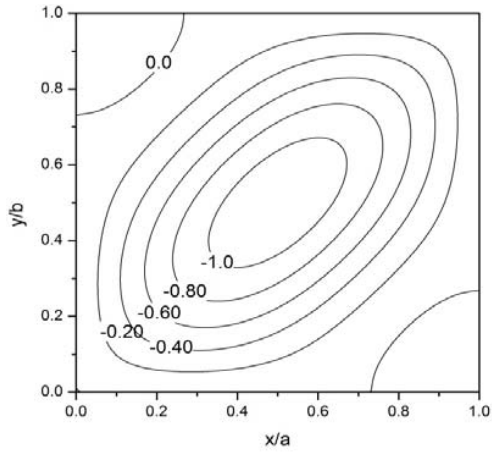

(a) 1st buckling mode

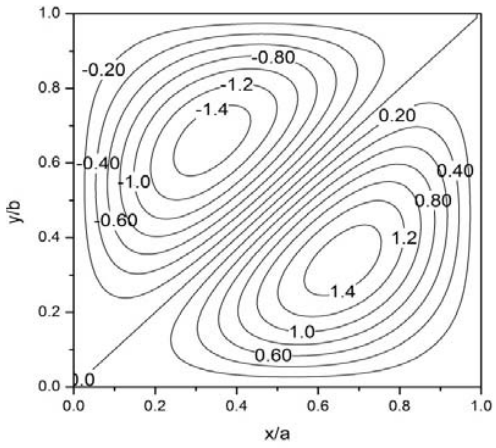

(b) 2nd buckling mode

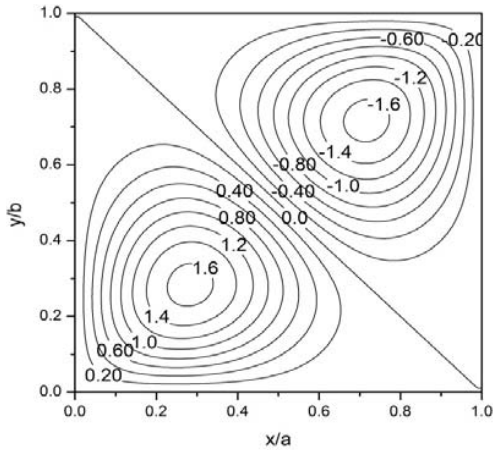

(c) 3rd buckling mode

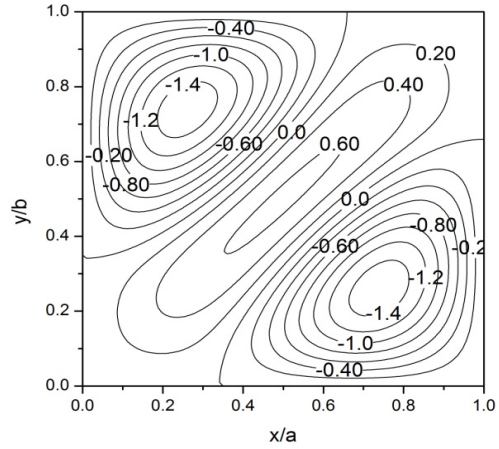

(d) 4th buckling mode

Fig. 9 Buckling mode shapes of a square plate subjected to uniformly distributed in-plane edge shear loads N_{xy}

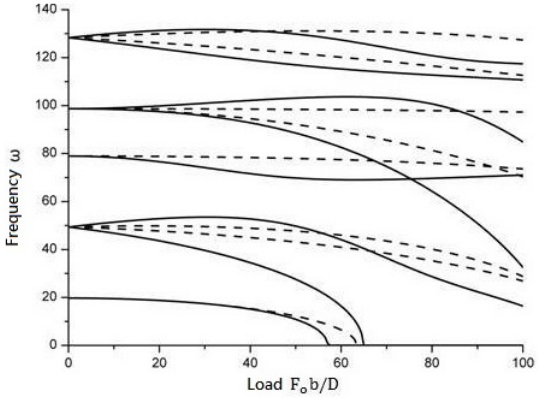

Fig. 10 Lowest eight natural frequency curves of a square plate subjected to two different locations of concentrated in-plane edge shear loads F_o

Solid curves: concentrated loads at $1/5$ of the edge length: Dash curves: concentrated loads at mid-points of all edges.

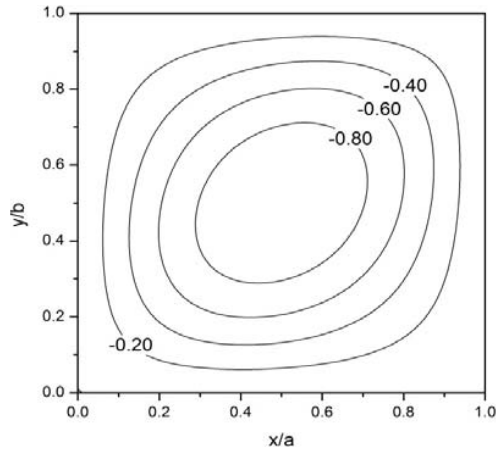

(a) 1st natural mode

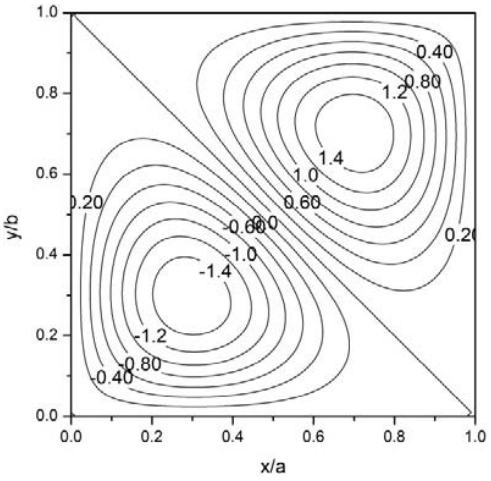

(b) 2nd natural mode

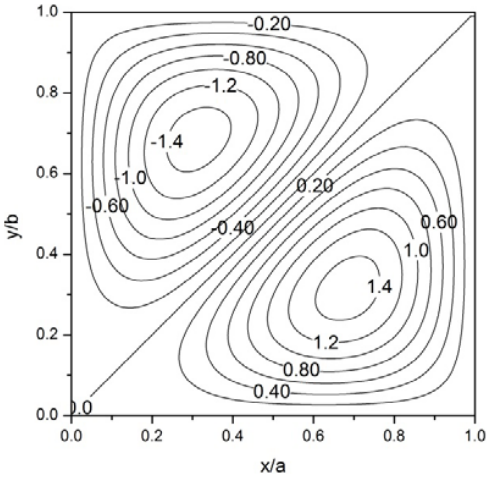

(c) 3rd natural mode

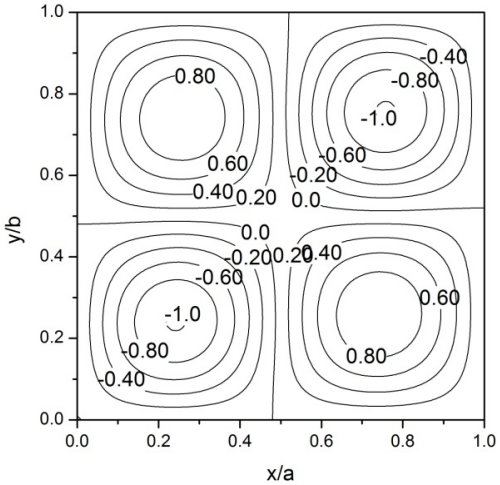

(d) 4th natural mode

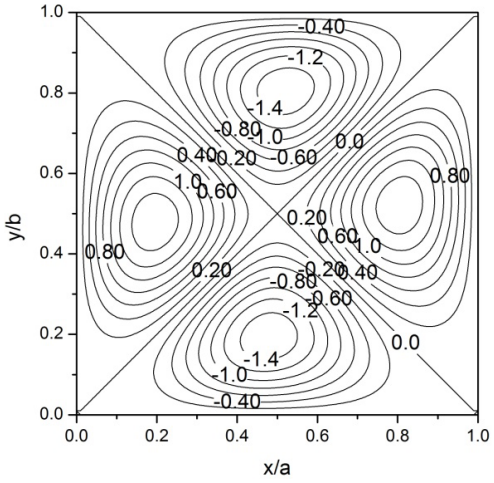

(e) 5th natural mode

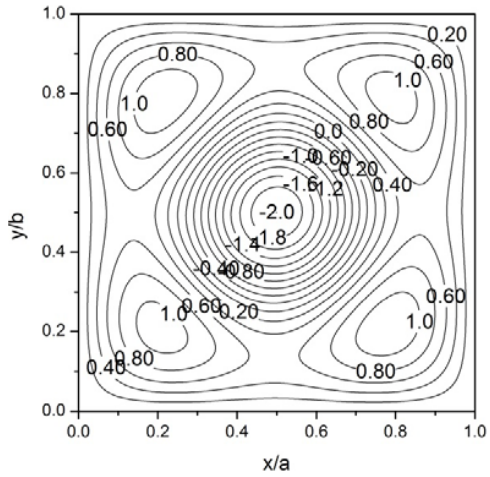

(f) 6th natural mode

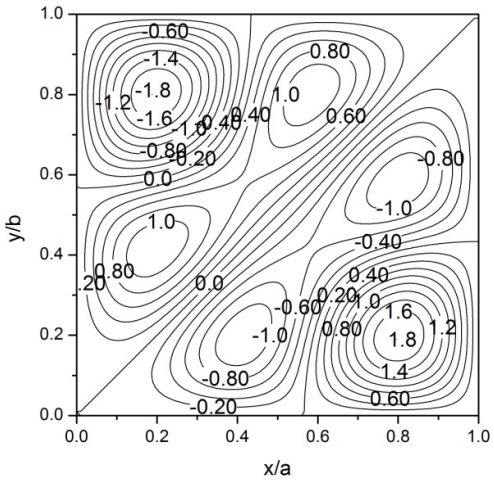

(g) 7th natural mode

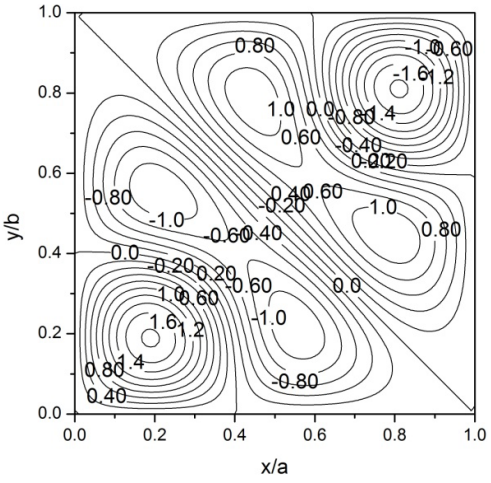

(h) 8th natural mode

Fig. 11 Natural mode shapes of a square plate subjected to concentrated in-plane edge shear loads F_o at the midpoints of all edges. $\frac{F_o b}{D}$=20

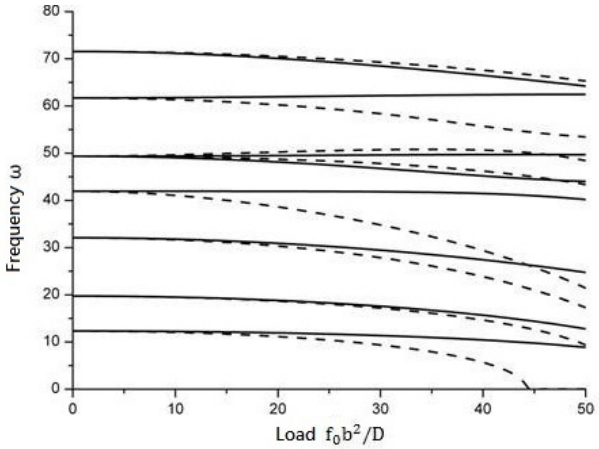

Fig. 12 Lowest eight natural frequency curves of a rectangular plate of aspect ratio $a/b = 2$ subjected to two different distributions of in-plane edge shear loads with the same resultants.

Solid curves: uniformly distributed loads: Dash curves: concentrated loads at mid-points of all edges.

REFERENCES

[1] A. W. Leissa, *Vibration of Plates*, NASA SP-160, 1969.
[2] N. Tahan, M. N. Pavlovic, and M. D. Kotsovos, "Single Fourier series solutions for rectangular plates under in-plane forces, with particular reference to the basic problem of collinear compression. Part 1: Closed-form solution and convergence study," *Thin-Walled Structures*, vol. 15, pp. 291-303, 1993.
[3] N. Tahan, M. N. Pavlovic, and M. D. Kotsovos, "Single Fourier series solutions for rectangular plates under in-plane forces, with particular reference to the basic problem of collinear compression. Part 1: Stress distribution," *Thin-Walled Structures*, vol. 17, pp. 1-26, 1993.
[4] J. H. Kang, and A.W. Leissa, "Exact solutions for the buckling of rectangular plates having linearly varying in-plane loading on two opposite simply supported edges," *International Journal of Solids and Structures*, vol. 42, pp. 4220-4238, 2005.
[5] O. Civalek, A. Korkmaz, and C. Demir, "Discrete singular convolution

approach for buckling analysis of rectangular Kirchhoff plates subjected to compressive loads on two-opposite edges," *Advances in Engineering Software*, vol. 41, pp. 557-560, 2010.

[6] A.V. Lopatin, and E. V. Morozov, "Buckling of the SSCF rectangular orthotropic plate subjected to linearly varying in-plane loading," *Composite Structures*, vol. 93, pp. 1900-1909, 2011.

[7] X. Wang, L. Gan, and Y. Zhang, "Differential quadrature analysis of the buckling of thin rectangular plates with cosine-distributed compressive loads on two opposite sides," *Advances in Engineering Software*, vol. 39, pp. 497-504, 2008.

[8] P. Jana, and K. Bhaskar, "Stability analysis of simply-supported rectangular plates under non-uniform uniaxial compression using rigorous and approximate plane stress solutions," *Thin-Walled Structures*, vol. 44, pp. 507-516, 2006.

[9] S. K. Panda, and L. S. Ramachandra, "Buckling of rectangular plates with various boundary conditions loaded by non-uniform in-plane loads," *International Journal of Mechanical Sciences*, vol. 52, pp. 819-828, 2010.

[10] Y. Tang, and X. Wang, "Buckling of symmetrically laminated rectangular plates under parabolic edge compressions," *International Journal of Mechanical Sciences*, vol. 53, pp. 91-97, 2011.

[11] Y. G. Liu, and M. N. Pavlovic, "A generalized analytical approach to the buckling of simply-supported rectangular plates under arbitrary loads," *Engineering Structures*, vol. 30, pp. 1346-1359, 2008.

[12] G. Ikhenazen, M. Saidani, and A. Chelghoum, "Finite element analysis of linear plates buckling under in-plane patch loading," *Journal of Constructional Steel Research*, vol. 66, pp. 11112-1117, 2010.

[13] X. Wang, L. Gan and Y. Wang, "A differential quadrature analysis of vibration and buckling of an SS-C-SS-C rectangular plate loaded by linearly varying in-plane stresses," *Journal of Sound and Vibration*, vol. 298, pp. 420-431, 2006.

[14] A. K. L. Srivastava, P. K. Datta, and A. H. Sheikh, "Buckling and vibration of stiffened plates subjected to partial edge loading," *International Journal of Mechanical Sciences*, vol. 45, pp. 73-93, 2003.

[15] S. M. Dickinson, "Lateral vibrations of rectangular plates subjected to in-plane forces," *Journal of Sound and Vibration*, vol. 16, pp. 465-472, 1971.

[16] J. P. Singh, and S. S. Dey, "Transverse vibration of rectangular plates subjected to in-plane forces by a difference based variational approach," *International Journal of Mechanical Sciences*, vol. 32, pp. 591-599, 1990.

[17] M. Azhari, S. Hoshdar, and M. A. Bradford, "On the use of bubble functions in the local buckling analysis of plate structures by the spline finite strip method," *International Journal for Numerical Methods in Engineering*, vol. 48, pp. 583-593, 2000.

[18] K. M .Liew, J. Wang, T. Y. Ng, and M. J. Tan, "Free vibration and buckling analyses of shear-deformable plates based on FSDT meshfree method," *Journal of Sound and Vibration*, vol. 276, pp. 997-1017, 2004.

[19] T. Q. Bui, M. N. Nguyen, and C. Zhang, "Buckling analysis of Reissner-Mindlin plates subjected to in-plane edge loads using a shear-locking-free and meshfree method," Engineering Analysis with Boundary Elements, vol. 35, pp. 1038-1053, 2011.